**NASA DEVELOP National Program**
**Pop-Up Project**

*Fall 2022*

# Shoshone River Water Resources

## Assessing Sediment Inputs into the Shoshone River in Wyoming to Determine Areas for Protection and Restoration Practices

**DEVELOP Technical Report**
Final Draft – November 17, 2022


Robyn Holmes (Project Lead)
Will Campbell
Cassie Ferrante
Nelson Lemnyuy

*Advisors:*
Dr. Austin Madson, University of Wyoming

*Fellow:*
Caroline Williams (Pop-Up Project)

# 1. Abstract

In 2016, a routine repair operation at the Willwood Dam released tons of built-up sediment into the Shoshone River, polluting the river and negatively impacting the ecosystem. This release greatly affected the communities that rely on the river for farming, recreation, and tourism. In partnership with the Wyoming Department of Environmental Quality (WYDEQ), Shoshone River Partners, and the United States Geological Survey (USGS) Wyoming–Montana Water Science Center, this project utilized satellite imagery and precipitation data to examine turbidity patterns in the Shoshone River between the Buffalo Bill Dam and the Willwood Dam. We used PlanetScope satellite images to assess changes in surface reflectance of the river in response to precipitation events and Global Precipitation Measurement (GPM) Integrated Multi-Spectral Retrieval (IMERG) precipitation data to estimate the lag time between rainfall events and increased turbidity. The National Land Cover Dataset (2019) was used to identify the main land cover types within each sub-basin. The end products included a turbidity analysis, land cover analysis, and precipitation analysis that provided the partners with a better understanding of sediment dynamics in the river. The results demonstrated the feasibility of using PlanetScope data to examine turbidity spatially along small rivers. Sediment plumes from tributaries were visually identified for multiple high turbidity events, and we calibrated an equation that translated reflectance to turbidity, accurately representing plume extent. Inconsistent spectral quality of PlanetScope data, however, limited our ability to assess the relative sediment contribution of the tributaries.



**Key Terms**

suspended sediment, tributaries, turbidity, precipitation, remote sensing, PlanetScope, GPM IMERG


# 2. Introduction

## *2.1 Background Information*

Rivers provide a myriad of important ecological and societal functions, including habitat, recreation, and water supply for irrigation. Excess suspended sediment impairs water quality and diminishes these functions; therefore, it is critical to monitor sources of excess sediment. In the Shoshone Basin, releases from the Willwood Dam have caused elevated sediment levels. Dams provide important water supply, flood control, and/or power generation services, however, the alteration of river processes causes collateral effects including the trapping and accumulation of sediments behind the dam. During routine dam maintenance, these sediments can be released all at once, having adverse effects on downstream water quality.

In 2016, a routine repair operation at the Willwood Dam released tons of built-up sediment into the Shoshone River, polluting the water downstream and causing a significant fish kill (Trosper, 2019). This release greatly concerned the communities that rely on the river for farming, recreation, and tourism. After the 2016 release, the Wyoming Department of Environmental Quality (WYDEQ) created the Willwood Working Groups to address community concerns over future sediment releases by improving aquatic habitat, working towards improved dam operation, and decreasing sediment loading through the implementation of Best Management Practices (BMPs).

The Willwood Working Group looking to implement BMPs focused their efforts on the reach of the Shoshone between the Buffalo Bill Dam and the Willwood Dam. The Buffalo Bill Dam is located upstream of the Willwood Dam. Limited sediment is released from the Buffalo Bill reservoir as it is large enough that most sediments settle out far away from the release gate. Between the Buffalo Bill Dam and Willwood Dam, several tributaries, irrigation canals, and channels feed into the river. Sediment transported by these tributaries accumulates behind the Willwood Dam before eventually being released.

This project assessed the feasibility of using PlanetScope satellite imagery to analyze turbidity patterns in a small river. The study area encompassed the Shoshone River watershed between the Buffalo Bill Dam and Willwood Dam (Figure 1). The Shoshone River area is situated in a valley surrounded by agricultural fields and small urban areas. Many creeks and ephemeral streams join the Shoshone River within the study area and

are known to transport high sediment loads, especially in response to storm events. One region of interest is the McCullough Peaks area, which contains highly erodible soil that may contribute to high sediment loading but is difficult to monitor due to the flashiness of its tributaries. To analyze turbidity patterns in the Shoshone River, we used PlanetScope imagery from January 2019 to October 2021 to remotely sense turbidity. The study period was selected to match the timeframe during which the United States Geological Survey (USGS) collected in-situ turbidity data within the study area so we would be able to calibrate the remote sensing data.

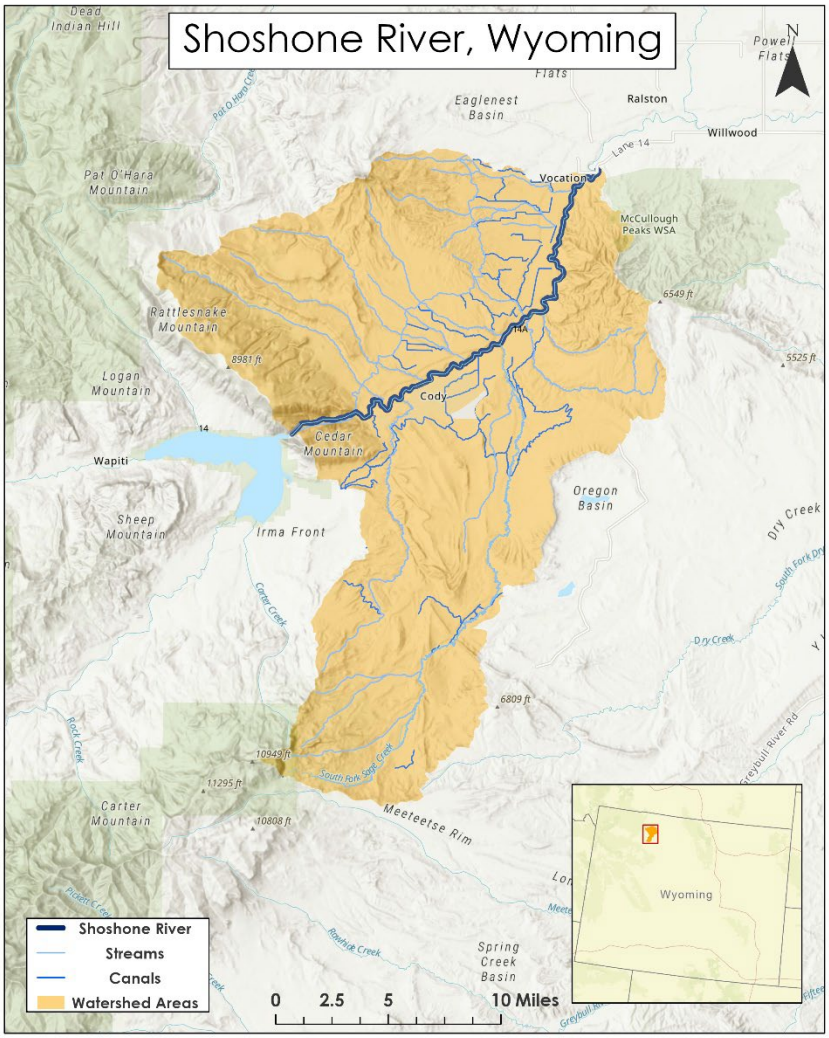


*Figure 1.* Map of the study area. The study area is highlighted in orange, rivers, streams, and canals are in blue. Basemap Citation: NRGC, Esri, HERE, Garmin, FAO, NOAA, USGS, EPA, Here, SafeGraph, METI/NASA, Bureau of Land Management, EPA, NPS. USDA, NASA, NGA.

### *2.2 Project Partners & Objectives*

We partnered with WYDEQ, the Shoshone River Partners (formerly known as Willwood Working Group 3), and the USGS Wyoming-Montana Water Science Center to investigate the sedimentary contributions of sub-watersheds and tributaries to the Shoshone River. These partner organizations have been conducting ongoing work to alleviate the impacts of excess sediment in the Shoshone River basin. Watershed managers in the working groups currently rely on in-situ turbidity data from the USGS stations and time-lapse photography to identify tributaries contributing high volumes of sediment to the Shoshone River. They use these discrete

sources of information to inform their BMPs within the watershed such as stream restoration and riparian fencing.

Based on the partner's identified needs, the primary objective was to assess the feasibility of using PlanetScope data to examine turbidity spatially along the Shoshone River. We supplemented the turbidity analysis with a precipitation analysis to estimate the lag time between rainfall events and increased turbidity. A land cover analysis was also conducted to identify the main land cover types within each sub-basin.

Remote sensing allows for the geospatial analysis of turbidity beyond what is possible with the partner's current in-situ data collection. This analysis improved the partners understanding of sediment dynamics in the Shoshone River, increased their ability to allocate their limited resources to implement BMPs effectively, and built their capacity to incorporate remote sensing in their management decisions.

## 3. Methodology

Many studies have successfully used remote sensing to determine surface water turbidity in rivers (Shen et al., 2021; Pereira et al., 2019; Hossain, 2021; Umar et al., 2018). Suspended sediment increases the reflection of certain wavelengths, allowing the surface reflectance recorded by multispectral satellite imagery to be used as a proxy for *in-situ* turbidity measurements. Red, green, and near infrared (NIR), or a combination of these are most commonly used to assess turbidity (Umar et al., 2018; Garg et al., 2020, Ayad et al., 2020). If adequate in-situ data are available, the reflectance-turbidity relationship can be calibrated, allowing for quantitative consideration of turbidity. In absence of in-situ data, the Normalized Difference Turbidity Index (NDTI) has been developed to look at relative turbidity within a study area and has been applied to multiple studies (Lacaux et al., 2007; Garg et al., 2020). Imagery for analyzing turbidity in rivers requires fine spatial resolution such that multiple pixels fit within a river cross section and fine temporal resolution to capture flood events before they dissipate. PlanetScope imagery has a 3m spatial resolution, daily temporal resolution, and has been shown to be effective at analyzing turbidity (Mansaray et al., 2021; Wirabumi et al., 2020). Past research has looked at spatial distribution of turbidity in large rivers, including sediment transport, mixing downstream of large river confluences, and sediment plumes from a single tributary (Hossain et al., 2021; Pereira et al, 2019; Umar et al 2018; Hughes et al., 2021); however, no studies were found over the course of this project's literature review that use remote sensing to identify tributaries contributing high sediment loading.

### *3.1 Data Acquisition*

We downloaded PlanetScope surface reflectance satellite images using Planet Explorer. Images from PlanetScope's first generation Dove Classic sensors were ignored as sensors do not provide as reliable imagery for spectral analyses (Frazier & Hemingway, 2021). We acquired turbidity data from a U.S. Geological Survey gage station on the Shoshone River above the Willwood Dam (USGS 06283995). GPM IMERG rainfall data were spatially averaged across the study area and downloaded as a daily time series through the Climate Engine application. For the land cover analysis, we downloaded USGS National Land Cover Database (NLCD) data from the National Geospatial Data Gateway. Project partners also provided us with a geodatabase containing watershed shapefiles and time-lapse imagery of select tributary confluences at 15-minute intervals.

### *3.2 Data Processing*

We first analyzed satellite rainfall data, gauge precipitation data, and turbidity data from January 2019 to October 2021 to identify dates of elevated turbidity and storm events. Turbidity and rainfall were plotted against time on a scatter plot to get a sense for the correlation between them. Turbidity and precipitation were also sorted by magnitude to find the dates of the largest precipitation and turbidity events. These dates were then used to search for images to be used as proof of concept for the rest of the project.

After confirming the ability to identify sediment plumes in PlanetScope imagery, we downloaded all usable images taken during the study period. We initially tried using Planet's surface normalized images; however, the normalization procedure caused the near infrared band to be higher in reflectance than the other bands

which interfered with NDWI masking. In order to apply our water masking method, we had to switch to using Top of Atmosphere (TOA) data and work with it un-normalized. We used the Python package gdal to merge the images taken during the same satellite pass. We then calculated the Normalized Difference Water Index (NDWI) (McFeeter, 1996):

$$\text{NDWI} = \frac{\text{Green - NIR}}{\text{Green + NIR}} \tag{1}$$

We used Otsu's method to determine a threshold value and convert NDWI to a binary raster which was used to mask land pixels, leaving just the river. The Python package rasterio was then used to create a mask based on Python's useable data mask image and apply it to the merged images, removing pixels where clearMap = 0, shadowMap = 1, lightHazeMap = 1, heavyHazeMap = 1, cloudMap = 1, or confidenceMap <80. Afterwards, the turbidity equation was applied to the raster image. Finally, a shapefile of the river was used to clip the resulting images to remove any land erroneously missed during NDWI masking.

We then calibrated multiple equations (Equations A1-A4, Appendix A) in order to find the best relationship between reflectance and turbidity. Band data was spatially averaged within a rectangle located adjacent to the USGS gage station using the rasterstats.zonal_stats function (Figure A1, Appendix A). A Python script retrieved in-situ turbidity for the nearest time to when the PlanetScope image was taken. If no turbidity was available within one hour of the image's timestamp, the image was not used for calibration and validation. The dataset was then sorted by the magnitude of turbidity. Entries with an even index were used for calibration while entries with an odd index were used for validation (where the first entry was indexed at zero). Parameters were calibrated using the basinhopping function from the SciPy.optimize package to minimize root mean squared error (RMSE) between remotely sensed and in-situ turbidity. The best fit was found using the Equation 2:

$$\text{T} = \frac{\text{GreenN}}{\text{a - b * RedN}} \tag{2}$$

Where,

$$\text{a} = 0.0451688$$

$$\text{b} = 0.157234$$

$$\text{GreenN} = \frac{\text{Green}}{\text{Red + Green + Blue + NIR}} \tag{2a}$$

$$\text{RedN} = \frac{\text{Red}}{\text{Red + Green + Blue + NIR}} \tag{2b}$$

T is turbidity, GreenN is green reflectance normalized to the sum all bands for the image pixel, and RedN is red reflectance normalized to the sum of all bands for each image pixel.

Equation 2 produced an $R^2$ of 0.83 for calibration, 0.22 for validation, and 0.70 for the full dataset. The Nash Sutcliffe Efficiency coefficient (NSE) for the full dataset was 0.70. A summary of parameters and $R^2$ values for the other equations and band combinations we tested can be found in Table 1A, Appendix A. Figure 2 shows that remotely sensed turbidity generally follows the same trends as in-situ turbidity; however, some peaks are missed. While this relationship generally does a good job of approximating turbidity, it tends to

overestimate low turbidity values and underestimate high turbidity values (Figure 3). The calibrated turbidity equation was then applied to the masked and trimmed PlanetScope images.

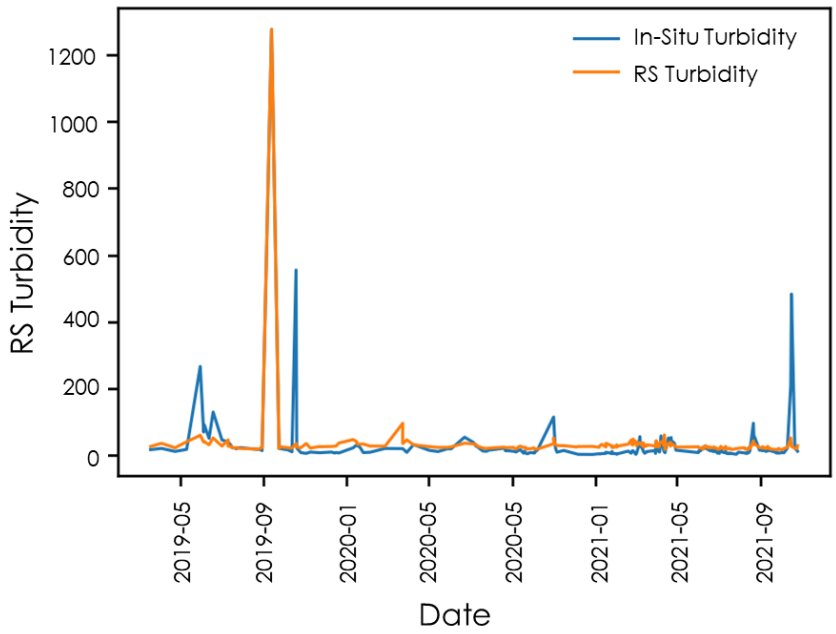


*Figure 2:* Remotely sensed and in-situ turbidity plotted for each usable image during the study period. In-situ turbidity is plotted in blue and remotely sensed (RS) turbidity is plotted in orange. Remotely sensed turbidity effectively models the turbidity spike on Sept. 12, 2019 but underestimates or misses many other peaks.

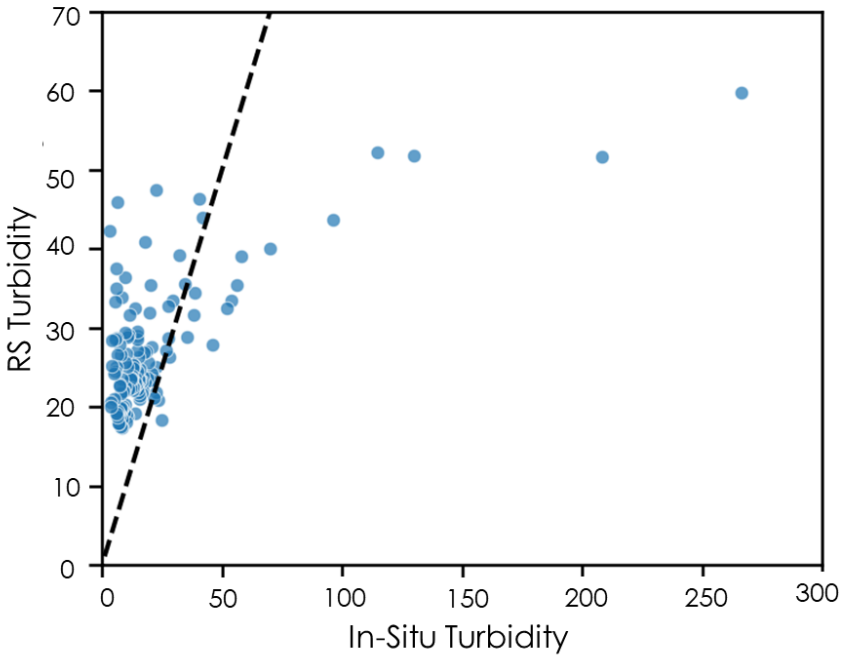


*Figure 3:* Remotely sensed vs in-situ turbidity for the validation dataset. ($R^2 = 0.22$) In-situ turbidity is plotted on the x-axis and remotely sensed (RS) turbidity is plotted on the y-axis. Each dot represents a satellite imaging event. In-situ turbidity was measured at the USGS gage above Willwood Dam. For each image the turbidity measurement with the nearest timestamp to when the image was used (within one hour either side).

The dashed line has a slope of 1 and intercept of 0, representing a perfectly modeled relationship. The majority of low in-situ values falling above this line and high values falling above it indicates the remote sensing turbidity equation frequently overestimates low turbidity and underestimates high turbidity.

### *3.3 Data Analysis*

We conducted a spatial analysis of turbidity by comparing remotely sensed turbidity at paired locations upstream and downstream of tributaries. Average remotely sensed turbidity was spatially extracted using zonal_stats function from the rasterstats package. We calculated percent land cover (NLCD) within each sub-basin using ArcGIS Pro v. 3.0.2 in order to identify the dominant land cover type for each sub-basin. We also analyzed rainfall events in order to forecast the amount of time it takes for sediment to be transported into the river following a storm.

Additionally, we conducted a precipitation trends analysis using GPM IMERG daily precipitation data and mean daily turbidity readings from the USGS streamflow station above Willwood Dam (06283995) from January 2019 to October 2021. After calculating a Pearson's correlation coefficient matrix in the Python using pandas.DataFrame.corr, we then squared the results to generate $R^2$ values among different time variables.

## 4. Results & Discussion

### *4.1 Analysis of Results*

To assess the feasibility of using PlanetScope data to map turbidity in the Shoshone River, we analyzed suspended sediment concentrations from 2019 to 2021. The analyses focused on remotely sensed turbidity, precipitation, and land cover. In-situ gage data from the USGS streamflow station provided a way to calibrate our remotely sensed turbidity findings. The land cover analysis provided additional context for turbidity patterns in the Shoshone River.

#### *4.1.1 Remotely Sensed Turbidity*

As a proof of concept that we could detect sediment plumes with PlanetScope data, we first visually identified sediment plumes in satellite images during the week following recent rainfall events. We observed visible sediment plumes from Sulphur Creek (upper watershed), Dry/Homesteader Creek (middle watershed), and Penney Gulch (lower watershed) on a clear PlanetScope image from September 12, 2019. These three confluences are known to contribute high volumes of sediment into the Shoshone River based on the Shoshone River Partner's StoryMap (Willwood Work Group 3, n.d.). This demonstrated that PlanetScope had a sufficient spatial resolution for our project, and that equation 2 successfully represented plumes seen on September 12th, 2019 (Figure 4) and October 16th, 2021 (Figures A2 and A3, Appendix A). The visible sediment plumes were later used to qualitatively validate the turbidity index (Figure 4, Figures A1 and A2 in Appendix A). The remotely sensed turbidity plume matches extent of an area of high turbidity seen in the RGBn image. Despite calibration and a reasonable spatial representation of turbidity, we recommend interpreting the turbidity index values as a relative scale until the index can be further refined as the turbidity index validation suggests the turbidity equation overestimates low turbidity and underestimates high turbidity (Figure 3).

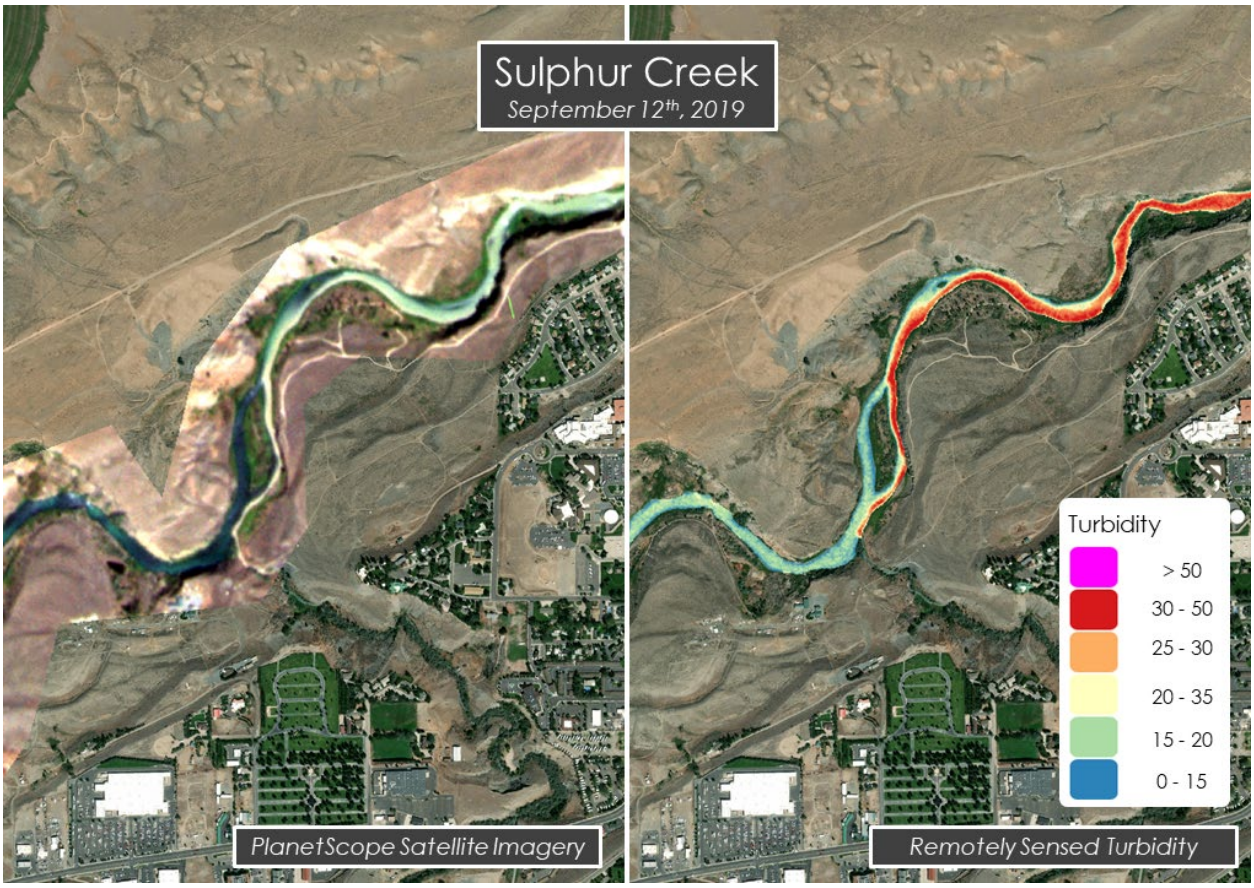


*Figure 4:* Comparison of remotely sensed turbidity and RGB imagery for a sediment plume at the confluence of Sulphur Creek and the Shoshone River on September 12th, 2019 (Both are overlaid on an Esri Satellite Basemap). Additional plume examples can be seen in Figures A1 and A2, Appendix A.

After confirming the relationship between reflectance and turbidity was meaningful, we were then able to use remotely sensed turbidity to attempt spatial analysis. In order to look for tributaries that contributed a high sediment load, we compared turbidity at paired locations upstream versus downstream (as illustrated in Figure A4, Appendix A). In theory, an increase in turbidity between the upstream and downstream locations should indicate that the tributary between the two locations contributed high sediment loading between the locations. In practice, however, large jumps in the value were mostly due to image inconsistences caused by clouds, land pixels, or image artifacts. Cloud masking, which we accomplished using the usable data mask provided by PlanetScope, was effective at removing thick clouds, however thin wispy clouds along the edge of thick clouds were sometimes missed (Figure A5, Appendix A). Rerunning image processing with a higher confidence level (we used 80%) may help get rid of this issue; however, we were unable to test it due to time constraints. Similarly, land masking using NDWI and river polygon clipping was for the most part effective at isolating water; however, in some cases it did not remove all land pixels. Further refinement of the automatic thresholding process would likely be able to reduce issues caused by land pixel interference.

We also attempted to look for a spatial pattern in turbidity by creating a box plot of turbidity at each of the downstream points to look at turbidity as the river flows through the study area. This faced the same issues as described in the last paragraph, so we were ultimately unable to reach a point where we had confidence in any quantitative spatial analysis results this term. Testing different shapes and locations to zonally extract along the river would also help ensure meaningful results. With these improvements, this analysis would be able to provide a different way to visualize turbidity along the river.

### *4.1.2 Land Cover Analysis*

We conducted a land cover analysis of each individual watershed using USGS National Land Cover Database (NLCD) from 2019 (Figure 5). We found that Shrub/Scrub made up the majority of most watersheds except for the Mainstream watershed and UnnamedTrib watershed that had less than 50% of their land cover comprised of Shrubs/Scrubs. Other landcover types that occupy significant portions in some watersheds are: Cultivated Lands, Hay/Pasture, Herbaceous, developed Low intensity, Evergreen Forest, and others occupying variable amounts (7% - 0%) of land cover in other watersheds include: Developed Open Space, Developed Medium Intensity, Barren Land, Deciduous Forest, Woody Wetlands, Emergent Herbaceous Wetlands, Open Water and Mixed Forest.

One limitation of this analysis may be that the most recent land cover data is from 2019. Once more updated land cover data becomes available, future studies should use that dataset to perform a land cover analysis.

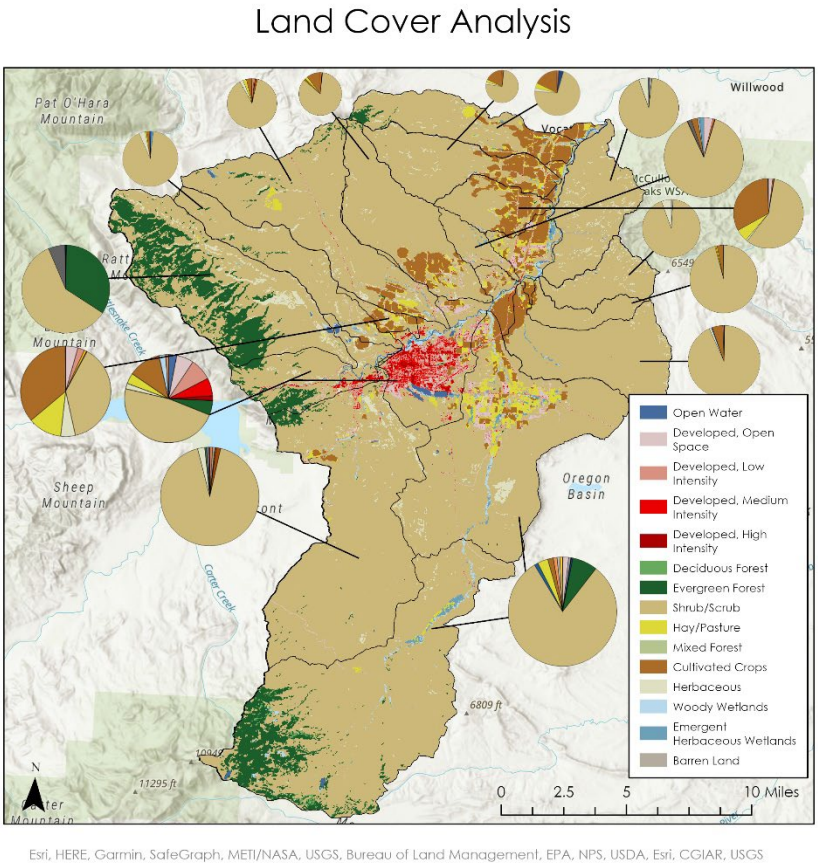


*Figure 5.* Map of the land cover analysis of the watersheds within the study area. The pie charts show the percentage of each land cover type per watershed.

Basemap Citation: Esri, HERE, Garmin, SafeGraph, METI/NASA, USGS, Bureau of Land Management, EPA, NPS, USDA, Esri, NASA, NGA.

### *4.1.3 Precipitation Trends Analysis*

Table 1 shows the GPM IMERG averaging time against mean daily turbidity from the USGS station. Averaging time was calculated by conducting a rolling average on the dataset in zero, two-day, or three-day intervals. The correlation between the variables was low, but we observed a higher correlation when comparing GPM IMERG precipitation data without snowmelt influence (only including the irrigation season between the months of April to October).

Table 1
*GPM IMERG Averaging Time Coefficient of Determination Matrix*

| **GPM IMERG Averaging Time** | **$R^2$, Without Snowmelt Influence (Apr to Oct)** | **$R^2$, Entire Study Period** |
|---|---|---|
| None | 0.14 | 0.12 |
| Two-Day | **0.37** | 0.32 |
| Three-Day | 0.35 | 0.31 |

We observed the highest correlation between mean two-day GPM IMERG data against mean daily turbidity (Figure 6). This finding is consistent with Alexander (2021) using mean two-day accumulated precipitation to compare precipitation against daily turbidity for the same precipitation above (Figure C2, Appendix C).

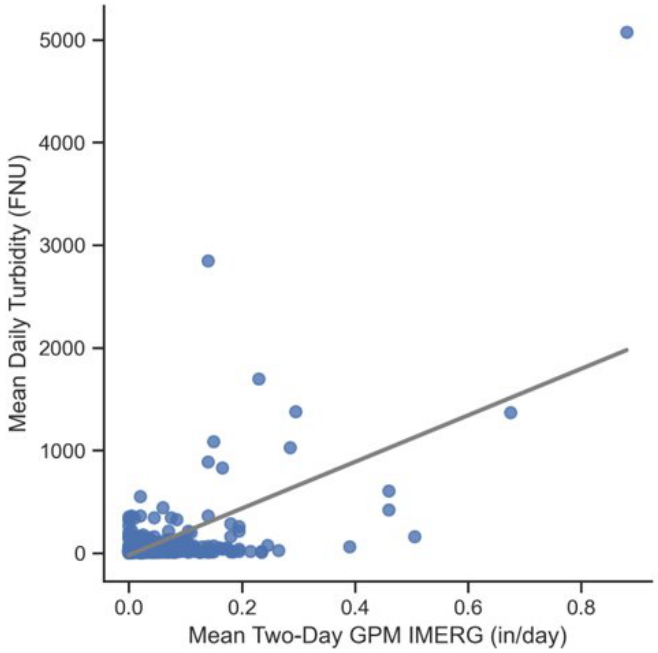


*Figure 6:* Mean Two-Day GPM IMERG data against Mean Daily Turbidity ($R^2$ = 0.37). Mean daily turbidity came from the USGS station above Willwood Dam. GPM IMERG data was a rolling two-day average.

To further examine when sediment is recorded in the monitoring station following a precipitation event, we generated a Pearson's correlation coefficient matrix examining GPM IMERG data at varying lag times against mean daily turbidity. Table 2 shows this relationship. Lag time was calculated by shifting the data values for precipitation back by one, two, or three days. The correlation between the variables was low, but we again observed a higher correlation when comparing GPM IMERG precipitation data without snowmelt influence.

Table 2
*GPM IMERG Lag Time Coefficient of Determination Matrix*

| GPM IMERG Lag Time | $R^2$, Without Snowmelt Influence (Apr to Oct) | $R^2$, Entire Study Period |
|---|---|---|
| One-Day | **0.35** | 0.30 |
| Two-Day | 0.05 | 0.05 |
| Three-Day | 0.01 | 0.01 |

We observed the highest correlation between One-Day GPM IMERG data against Mean Daily Turbidity (Figure 7). This finding also supports that turbidity is reflected in the monitoring station after at least a day after a storm event.

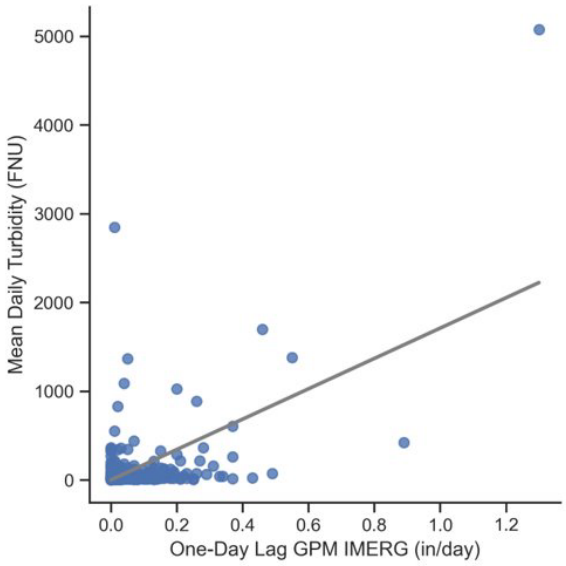


*Figure 7.* One-Day Lag GPM IMERG data against Mean Daily Turbidity ($R^2$ = 0.35) Mean daily turbidity came from the USGS station above Willwood Dam. GPM IMERG data was shifted by one day.

Both correlation matrices support a higher correlation between precipitation and turbidity when eliminating seasons with a high likelihood of snowmelt triggered events. They both support the finding that sediment takes at least a day to show up in the turbidity gage readings after precipitation falls on the watershed. However, even the best correlations demonstrate a relatively weak correlation, and so more research would need to examine if these trends are found exploring different datasets, time differences, or other factors that might improve the correlation between these variables.

We recommend that the second term explore other precipitation datasets with higher spatial resolution. We found that GPM IMERG and Parameter-elevation Regressions on Independent Slopes Mode (PRISM) data are somewhat comparable (Figure C1, Appendix C), but PRISM or Community Collaborative Rain, Hail & Snow Network (CoCoRaHS) data may be better alternatives to examine precipitation spatially and to explore the differences between the snowmelt season and off-season more in detail. Higher resolution spatial data could also allow the second term to investigate precipitation on the left and right banks of the river, or within each sub-basin, to further refine the relationship and to combine these findings with land cover types or soil moisture metrics to generate a better understanding of sediment dynamics within each sub-basin for the partners.

In addition, it might be worthwhile to create a threshold to exclude rainfall below a certain number, which might lead to a better correlation between the data. Alexander (2021) generated a higher correlation coefficient when examining rainfall depth above 0.01mm (Figure C2, Appendix C). In addition, Alexander (2021) used PRISM and CoCoRaHS data which may also explain the higher correlation between the datasets. It also might be worth exploring if a logistic regression or another type of regression fits the relationship better after these changes are made. Due to time constraints, we were not able to explore these relationships, but these could direct the second term's course of action.

### *4.2 Future Work*

The second term of this project will focus on a snow cover analysis. The future team will analyze the influence of large snowfall and melt events on sediment runoff. They will use the Soil Water & Assessment Tool (SWAT) to explore these trends in the Shoshone River. An additional objective is to quantify the amount of sediment from each tributary. The future team can reference the equation we derived and resolve the spectral quality issues with PlanetScope data in order to find a consistent relationship between turbidity and TOA radiance. Applying atmospheric normalization to the TOA radiance images may improve performance of NDWI masking and turbidity extraction. There is also plenty of room to expand on our attempts at spatial analysis. Our calibrated equation worked better on days with high turbidity, but we were unable to standardize our relationship among different days. The anticipated end products will include snow cover analysis maps as well as quantitative sediment contribution maps.

Future work could also investigate additional research questions that the partners were interested in, such as examining the contribution from McCullough Peaks. Precipitation datasets with higher spatial resolution may help that team isolate the sediment contribution to the McCullough Peaks sub-basin. The second term can also investigate irrigation practices more in depth, such as examining if irrigation return flows from nearby canals influence sediment runoff. Although we considered the irrigation season and snowmelt influence as a potential factor for the precipitation trends analysis, the second term could explore this variable in relation to sediment loading.

## 5. Conclusions

This project demonstrated the potential for PlanetScope data to be used to examine turbidity spatially along small rivers. We were able to identify multiple sediment plumes caused by tributaries joining the Shoshone River. This is relevant to watershed managers looking to identify sources of sediment and to target their best management practices along the river. We successfully ran an equation that translated the TOA radiance from the PlanetScope satellite images to turbidity, but the spectral quality of the data prevented us from finding a consistent relationship between turbidity and TOA radiance across the entire study period. Furthermore, the land cover analysis map we created can be used by the partners to understand how the different land cover types influence sediment contribution into the Shoshone River. Based on this research, future studies can refer to the equations and methods we derived for our turbidity analysis along small rivers. We also recommend any future work to include using a precipitation dataset with a higher spatial resolution, such as PRISM or CoCoRaHS, to analyze precipitation patterns within each sub-basin in combination with the land cover analysis.

## 6. Acknowledgments

The Shoshone River Water Resources team would like to thank our partners from the WYDEQ, the Shoshone River Partners, and the USGS for their collaboration and guidance on this project. We also would like to express our gratitude to our science advisor Dr. Austin Madson, and to our fellow Caroline Williams for their input and guidance throughout the project's duration. Thank you to Laramie Plott and Cecil Byles of the Project Coordination team as well for editing our deliverables and providing feedback.

This work utilized data made available through the NASA Commercial Smallsat Data Acquisition (CSDA) program. PlanetScope Imagery courtesy of Planet Labs, Inc.



Any opinions, findings, and conclusions or recommendations expressed in this material are those of the author(s) and do not necessarily reflect the views of the National Aeronautics and Space Administration.

This material is based upon work supported by NASA through contract NNL16AA05C.

## 7. Glossary

**Confluence** – The junction of two rivers
**CSS** – Concentration of Suspended Sediment
**Earth observations** – Satellites and sensors that collect information about the Earth's physical, chemical, and biological systems over space and time
**ESA** – European Space Agency
**GPM IMERG** – Global Precipitation Measurement (Integrated Multi-satellitE Retrievals). An algorithm that estimates the precipitation over Earth using the GPM satellite.
**gSSURGO** – Gridded Soil Survey Geographic Database
**NDTI** – Normalized Difference Turbidity Index. Identifies water turbidity using the ratio of green to red bands, as clear water has a higher electromagnetic reflectance in the green spectrum.
**NDWI** – Normalized Difference Water Index. Identifies water bodies as water has a higher electromagnetic reflectance in the Green and Near Infrared bands.
**NIR** – Near-infrared part of the electromagnetic spectrum between 215 to 400 THz.
**NLCD** – National Land Cover Database
**PlanetScope** – 3m resolution 8-band satellite imagery operated by Planet Labs
**Turbidity** – The measure of light scatter due to suspended particles.
**USDA-NRCS** – United States Department of Agriculture-National Resource Conservation Service
**USGS** – United States Geological Survey

## 8. References


Alexander, J. (2021). Quantifying Fine Sediment Dynamics in the Shoshone River Around Willwood Dam, Park County, Wyoming. *Wyoming-Montana Water Science Center.*

Ayad, M., Li, J., Holt, B., & Lee, C. (2020). Analysis and classification of stormwater and wastewater runoff from the Tijuana River using remote sensing imagery. *Frontiers in Environmental Science, 8*, 599030. https://doi.org/10.3389/fenvs.2020.599030

Frazier, A. E. & Hemingway, B. L. (2021) A Technical Review of Planet Smallsat Data: Practical Considerations for Processing and Using PlanetScope Imagery. *Remote Sensing 13*, 3930. https://doi.org/10.3390/rs13193930

Garg, V., Aggarwal, S. P., & Chauhan, P. (2020). Changes in turbidity along Ganga River using Sentinel-2 satellite data during lockdown associated with COVID-19. *Geomatics, Natural Hazards and Risk, 11*(1), 1175-1195. https://doi.org/10.1080/19475705.2020.1782482

Hossain, A.K.M.A., Mathais, C., Blanton, R. (2021) Remote Sensing of Turbidity in the Tennessee River Using Landsat 8 Satellite. *Remote Sensing, 14*, 3785. https://doi.org/10.3390/rs13183785

Huffman, G.J.,Stocker, E.F. , Bolvin, D.T. , Nelkin, E.J., & Tan, J. (2019). GPM IMERG Final Precipitation L3 Half Hourly 0.1 degree x 0.1 degree V06, Greenbelt, MD, Goddard Earth Sciences Data and Information Services Center (GES DISC). https://doi.org/10.5067/GPM/IMERG/3B-HH/06

Lacaux, J. P., Tourre, Y. M., Vignolles, C., Ndione, J. A., & Lafaye, M. (2007). Classification of ponds from high-spatial resolution remote sensing: Application to Rift Valley Fever epidemics in Senegal. *Remote Sensing of Environment, 106*(1), 66-74. https://doi.org/10.1016/j.rse.2006.07.012

Mansaray, A. S., Dzialowski, A. R., Martin, M. E., Wagner, K. L., Gholizadeh, H., & Stoodley, S. H. (2021). Comparing PlanetScope to Landsat-8 and Sentinel-2 for Sensing Water Quality in Reservoirs in Agricultural Watersheds. *Remote Sensing, 13*(9), 1847. https://doi.org/10.3390/rs13091847

McFeeters, S.C. (1996) The use of Normalized Difference Water Index (NDWI) in the delineation of open water features. *International Journal of Remote Sensing 17*(7) 1425-1432. https://doi.org/10.1080/01431169608948714

Pereira, F. J. S., Costa, C. A. G., Foerster, S., Brosinsky, A., & de Araújo, J. C. (2019). Estimation of suspended sediment concentration in an intermittent river using multi-temporal high-resolution satellite imagery. *International Journal of Applied Earth Observation and Geoinformation, 79*, 153-161. https://doi.org/10.1016/j.jag.2019.02.009

Planet Team (2022). Planet Application Program Interface: In Space for Life on Earth. San Francisco, CA. https://www.api.planet.com

Shen, M., Wang, S., Li, Y., Tang, M., & Ma, Y. (2021). Pattern of turbidity change in the middle reaches of the Yarlung Zangbo River, Southern Tibetan Plateau, from 2007 to 2017. *Remote Sensing, 13*(2), 182. https://doi.org/10.3390/rs13020182

Trosper, A. (2019). A Collaborative Effort Among Partners to Address Sediment Contributions to the Shoshone River. Powell-Clarks Fork Conservation District (PCFCD). https://www.usbr.gov/watersmart/cwmp/docs/2019/applications/CWMP1%20-%20003%20Powell%20Clarks%20Fork%20Conseration%20District_508.pdf

Umar, M., Bruce L. Rhoads, and Jonathan A. Greenberg. (2018) Use of multispectral satellite remote sensing to assess mixing of suspended sediment downstream of large river confluences. *Journal of Hydrology 556* 325-338. https://doi.org/10.1016/j.jhydrol.2017.11.026

Willwood Work Group 3. (n.d.). Working Together to Protect the Shoshone River. Retrieved November 8, 2022, from https://arcg.is/1ymq19

# 9. Appendix

**Appendix A:** *Turbidity Equation Calibration and Validation*

$$T = a * Band1 + b * Band2^2 \quad (A1)$$

*Equation A1:* Double band equation, format equivalent to equation "DSB1" in Pereira et al. 2019.

$$T = \frac{Band1}{a + b * Band2} \quad (A2)$$

*Equation A2:* Double band equation, format equivalent to equation "DSB3" in Pereira et al. 2019.

$$T = \frac{Band1}{a + b * Band2^2} \quad (A3)$$

*Equation A3:* Double band equation, format equivalent to equation "DSB3" in Pereira et al. 2019.

$$T = a * \frac{(Band1 + Band2)}{2} + b \quad (A4)$$

*Equation A4:* Double band equation.

*Table A1:* Summary of turbidity equation fitting results. The highlighted row represents the best fit equation which was used for spatial turbidity analysis.

| Equation Format | **Band Combination** | **a** | **b** | **$R^2$ (calibration)** | **$R^2$ (validation)** | **$R^2$ (all)** | **NSE (all)** |
|---|---|---|---|---|---|---|---|
| Eqn1 | red-green | 634.4853 | -1115.87 | 0.053162 | 0.030774 | 0.041898 | 0.035583 |
| Eqn2 | red-green | 0.007285 | -0.00578 | 0.173637 | 0.157548 | 0.155382 | 0.018806 |
| Eqn3 | red-green | 0.006125 | -0.00626 | 0.163368 | 0.144969 | 0.145441 | 0.018657 |
| Eqn4 | red-green | 33.05265 | -12.185 | 0.254587 | 0.07459 | 0.201443 | 0.173938 |
| Eqn1 | green-red | -462.603 | 3750.363 | 0.129206 | 0.089121 | 0.107899 | 0.096597 |
| **Eqn2** | **green-red** | **0.04705** | **-0.16382** | **0.830359** | **0.222667** | **0.700251** | **0.699771** |
| Eqn3 | green-red | 0.026758 | -0.32475 | 0.829276 | 0.228016 | 0.697286 | 0.696755 |
| Eqn4 | green-red | -12.185 | 33.05265 | 0.254587 | 0.07459 | 0.201443 | 0.173938 |
| Eqn1 | red-nir | 382.2884 | -1959.97 | 0.046855 | 0.06383 | 0.046265 | 0.034639 |
| Eqn2 | red-nir | 0.005456 | 0.000812 | 0.148141 | 0.128436 | 0.13116 | 0.018534 |
| Eqn3 | red-nir | 0.005282 | 0.013055 | 0.157692 | 0.147417 | 0.142641 | 0.018889 |
| Eqn4 | red-nir | 26.43944 | -12.2684 | 0.280252 | 0.2123 | 0.255578 | 0.170158 |
| Eqn1 | nir-red | -1170.58 | 4514.287 | 0.156215 | 0.154387 | 0.143773 | 0.133682 |
| Eqn2 | nir-red | 0.024106 | -0.0839 | 0.819182 | 0.079681 | 0.683151 | 0.682965 |
| Eqn3 | nir-red | 0.014386 | -0.17457 | 0.819194 | 0.072261 | 0.68137 | 0.681367 |
| Eqn4 | nir-red | -12.2684 | 26.43944 | 0.280252 | 0.2123 | 0.255578 | 0.170158 |
| Eqn1 | green-nir | 95.02479 | 262.2209 | 0.000274 | 0.002418 | 0.000702 | -0.00282 |

| | | | | | | | |
|---|---|---|---|---|---|---|---|
| Eqn2 | green-nir | 0.011842 | -0.02125 | 8.76E-05 | 0.000823 | 0.000259 | -0.00265 |
| Eqn3 | green-nir | 0.009932 | -0.0542 | 0.000281 | 0.00014 | 0.000226 | -0.00261 |
| Eqn4 | green-nir | 8.348716 | 7.012771 | 0.000163 | 0.002447 | 0.000622 | -0.00469 |
| Eqn1 | nir-green | 125.6434 | 175.8622 | 3.50E-05 | 0.005086 | 0.000698 | -0.00338 |
| Eqn2 | nir-green | 0.010233 | -0.01991 | 1.80E-06 | 0.004887 | 0.000441 | -0.00492 |
| Eqn3 | nir-green | 0.007115 | -0.0315 | 4.07E-08 | 0.005439 | 0.000533 | -0.00515 |
| Eqn4 | nir-green | 7.01277 | 8.348717 | 0.000163 | 0.002447 | 0.000622 | -0.00469 |
| Eqn1 | blue-red | -462.357 | 4162.696 | 0.169357 | 0.124933 | 0.143744 | 0.128732 |
| Eqn2 | blue-red | 0.057377 | -0.20004 | 0.825047 | 0.173815 | 0.690685 | 0.690599 |
| Eqn3 | blue-red | 0.032117 | -0.39068 | 0.824414 | 0.174409 | 0.688374 | 0.688257 |
| Eqn4 | blue-red | -25.6313 | 48.34161 | 0.809532 | 0.124264 | 0.68483 | 0.668621 |
| Eqn1 | red-blue | 990.4434 | -1506.42 | 0.134765 | 0.104445 | 0.114567 | 0.101005 |
| Eqn2 | red-blue | -0.03173 | 0.122638 | 0.817884 | 0.024148 | 0.667712 | 0.667309 |
| Eqn3 | red-blue | -0.01427 | 0.213485 | 0.817068 | 0.02316 | 0.664813 | 0.664029 |
| Eqn4 | red-blue | 48.34161 | -25.6313 | 0.809532 | 0.124264 | 0.68483 | 0.668621 |
| Eqn1 | blue-nir | 26.05916 | 1025.978 | 0.000776 | 0.009247 | 0.002208 | -0.01419 |
| Eqn2 | blue-nir | 0.013715 | -0.01879 | 0.20451 | 0.159322 | 0.170854 | -0.0147 |
| Eqn3 | blue-nir | 0.012002 | -0.04692 | 0.200262 | 0.149111 | 0.165623 | -0.01463 |
| Eqn4 | blue-nir | 2.692731 | 15.53078 | 0.004055 | 0.013001 | 0.005605 | -0.02906 |
| Eqn1 | nir-blue | 538.6 | -406.388 | 0.013281 | 0.001637 | 0.007631 | -0.00418 |
| Eqn2 | nir-blue | -0.02617 | 0.10094 | 0.809043 | 0.004327 | 0.64769 | 0.644442 |
| Eqn3 | nir-blue | -0.01196 | 0.178053 | 0.808667 | 0.004549 | 0.645192 | 0.640838 |
| Eqn4 | nir-blue | 15.53077 | 2.692732 | 0.004055 | 0.013001 | 0.005605 | -0.02906 |
| Eqn1 | blue-green | -484.277 | 2217.506 | 0.024742 | 0.027584 | 0.022375 | 0.012669 |
| Eqn2 | blue-green | 0.002892 | 0.027169 | 0.144235 | 0.093182 | 0.109999 | -0.01458 |
| Eqn3 | blue-green | 0.006316 | 0.052403 | 0.133385 | 0.086848 | 0.101513 | -0.01457 |
| Eqn4 | blue-green | -76.9736 | 92.69536 | 0.813725 | 0.001715 | 0.061161 | -7.0781 |
| Eqn1 | green-blue | 1403.738 | -3256.18 | 0.137622 | 0.09968 | 0.109323 | 0.085007 |
| Eqn2 | green-blue | -0.04123 | 0.159141 | 0.817697 | 0.017618 | 0.66627 | 0.666079 |
| Eqn3 | green-blue | -0.01824 | 0.272111 | 0.817274 | 0.017467 | 0.663509 | 0.663141 |
| Eqn4 | green-blue | 92.69536 | -76.9736 | 0.813725 | 0.001715 | 0.061161 | -7.0781 |

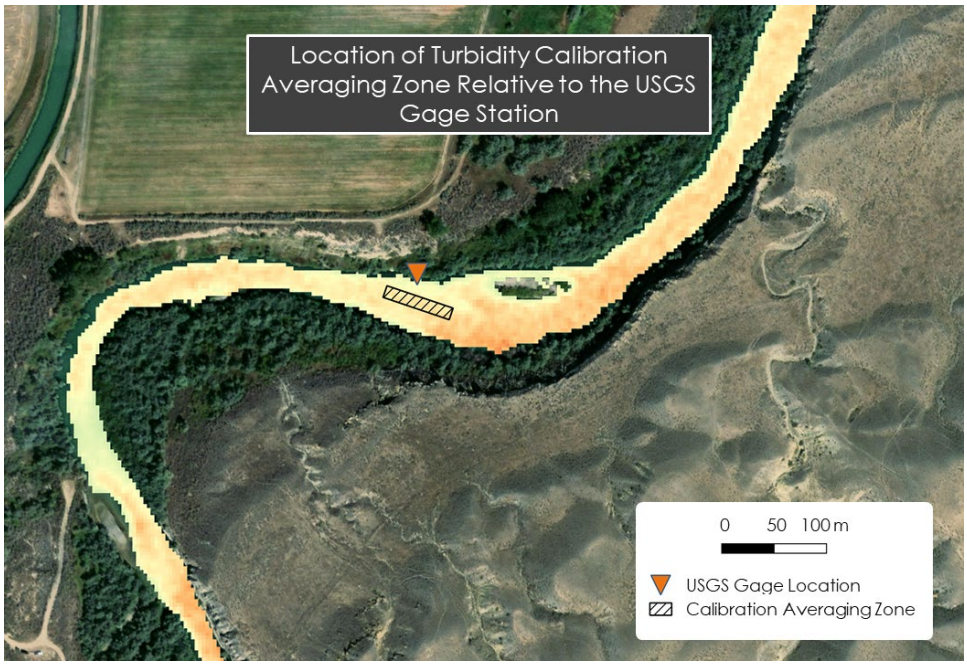


*Figure A1:* Location of Turbidity Calibration Averaging Zone Relative to the USGS Gage Station. The averaging zone was used to extract the average value for the red, green, blue, and near-IR bands in each image. These values were then used to calibrate the turbidity index equation.

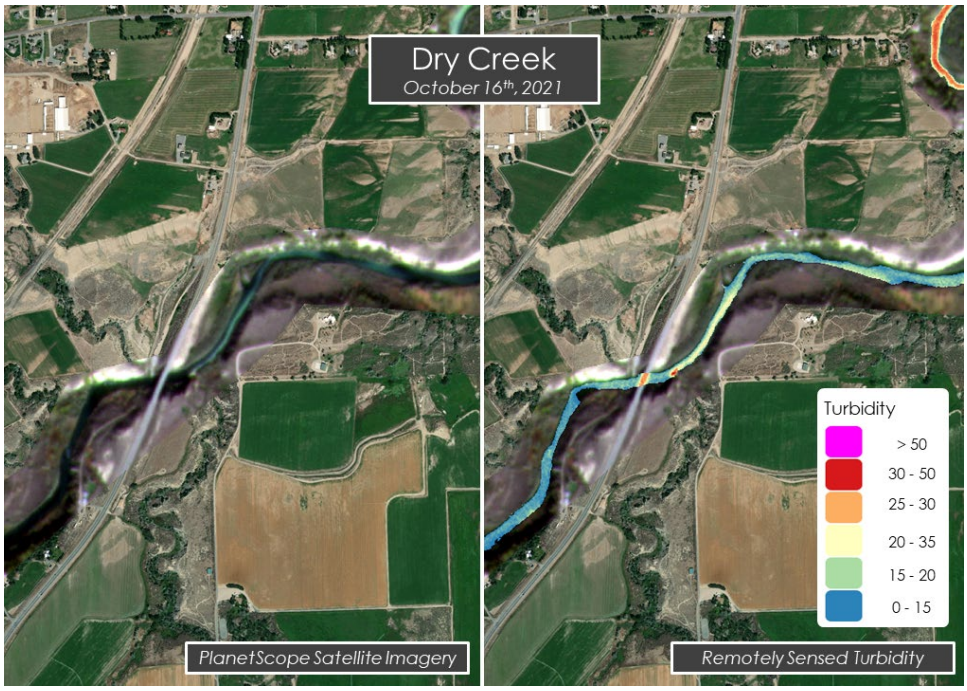


*Figure A2:* The map on the left shows raw PlanetsScope satellite imagery of a sediment plume at the confluence of Dry Creek on October 16th, 2021 (overlaid on an Esri Satellite basemap), the map on the right shows the turbidity index. The turbidity index accurately represents the extent of both of these plumes.

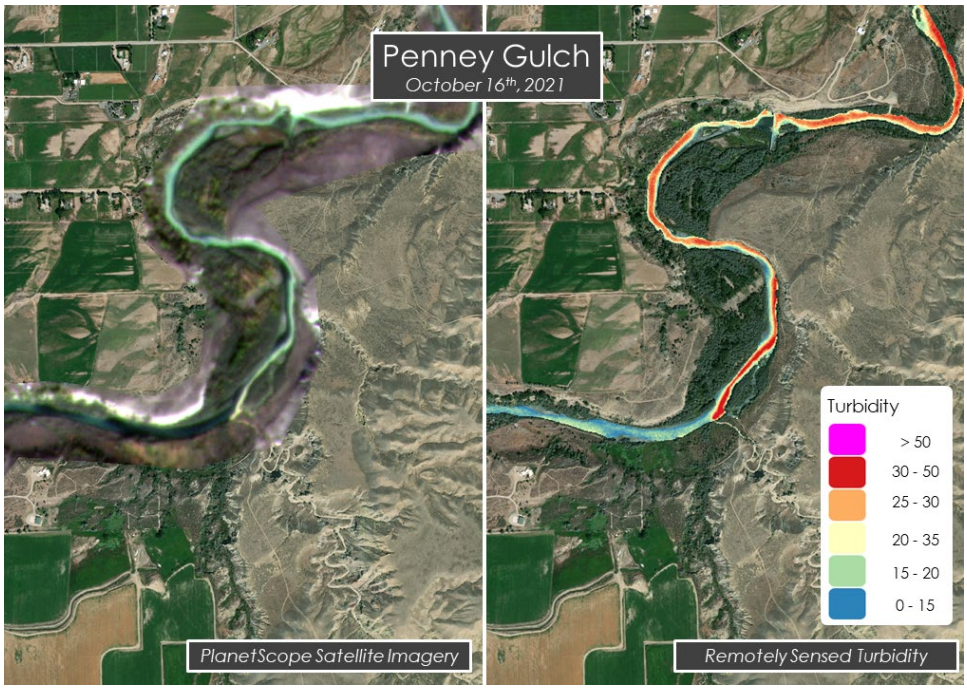


*Figure A3:* The map on the left shows raw PlanetScope satellite imagery of a sediment plume at the confluence of Penney Gulch on October 16th, 2021 (overlaid on an ESRI Satellite basemap), and the map on the right shows the turbidity index. The turbidity index accurately represents the extent of both of these plumes.

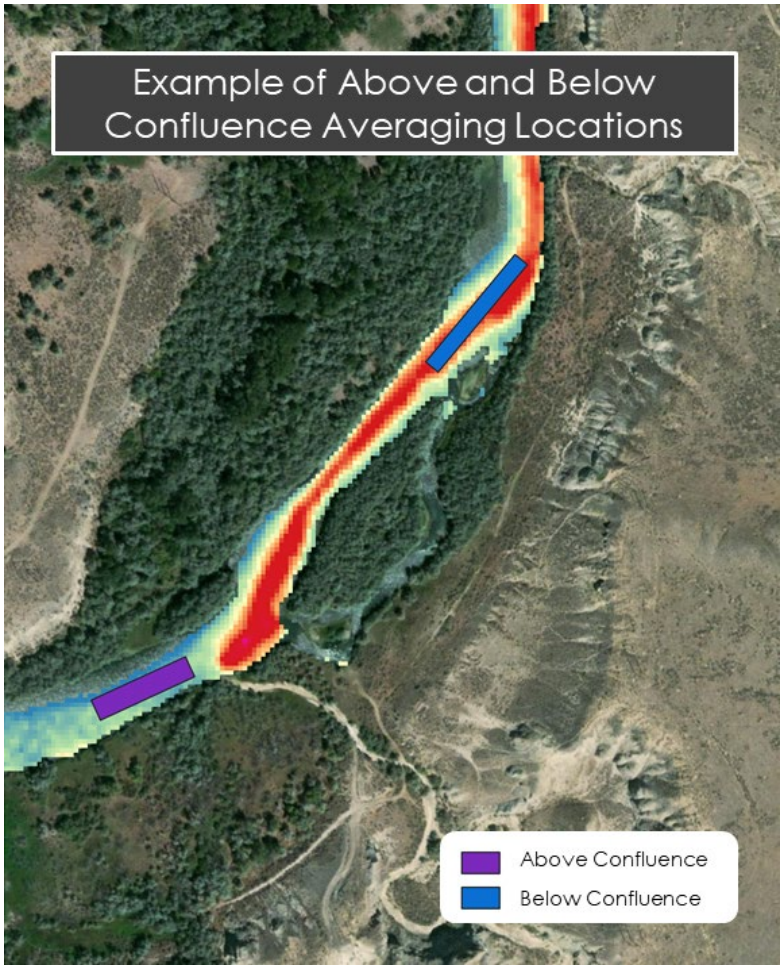


*Figure A4:* This map illustrates how using boxes above and below a confluence to get a zonal average turbidity should be able to detect an increase in turbidity due to a sediment-laden tributary joining the main stem Shoshone.

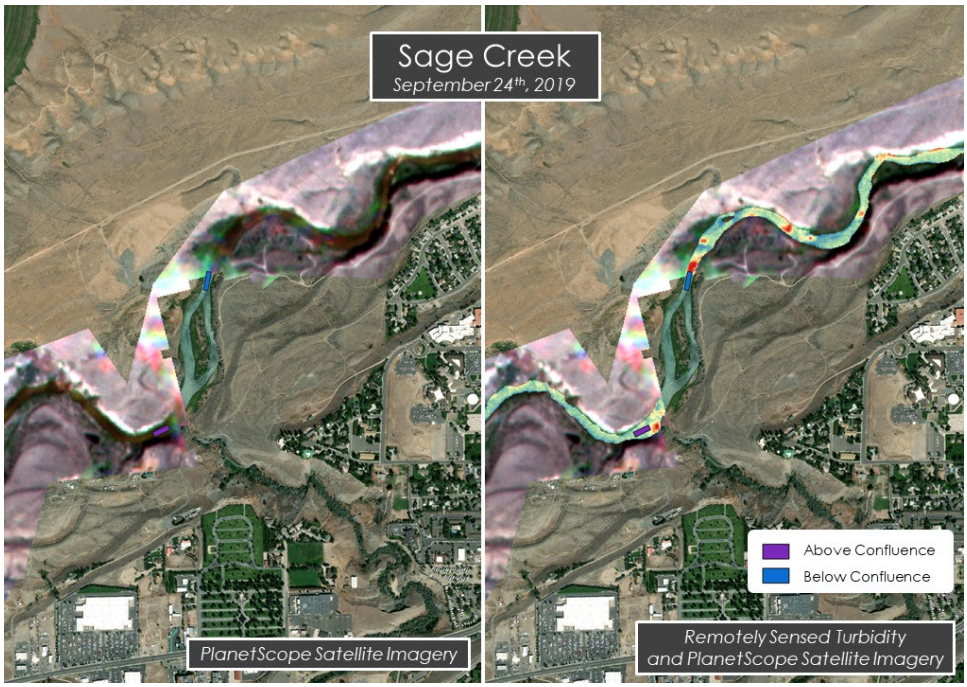


*Figure A5:* An example of clouds interfering with sediment plume detection at the confluence of Sage Creek on September 24th, 2019. The image on the left shows the raw PlanetScope imagery overlaid on an Esri satellite basemap. There is a missing rectangle of PlanetScope image because it was removed during cloud masking, however there are still some thin wispy clouds that weren't removed creating image inconsistencies. The Above-Below boxes are also shown to illustrate how this caused issues with comparing upstream vs downstream turbidity values.

**Appendix B:** *Land Cover Classification Types*

*Table B1:* Summary of landcover types within each subwatershed.

| **Sub-Basin** | **Shrub/ Scrub (%)** | **Cultivated Land (%)** | **Hay/Pasture (%)** | **Herbaceous (%)** | **Developed Low intensity (%)** | **Evergreen Forest (%)** |
|---|---|---|---|---|---|---|
| Trail-Creek-watershed | 59 | <1 | <1 | 6 | <1 | 34.3 |
| BuckCreek-watershed | 72 | 17 | 4.4 | 2.2 | <1 | 3.3 |
| SageCreek-watershed | 81.81 | 2.2 | 3.3 | 1.1 | <1 | 8.8 |
| Cottonwood-watershed | 89 | 3 | 2.2 | 2.2 | 1.1 | 1.2 |
| DryCreek-HomesteadCreek-watershed | 92.9 | 4.7 | <1 | 1.0 | <1 | <1 |
| DryCreek-watershed | 91.7 | 1.6 | <1 | 3.5 | <1 | 1.3 |
| DryGulch-watershed | 88.4 | 2.7 | 1.6 | <1 | <1 | 0 |
| IdahoCreek-watershed | 84.5 | 10.3 | 2 | 1.3 | <1 | <1 |
| IronCreek-watershed | 74.4 | 17.7 | 2.6 | 2.2 | <1 | <1 |
| Mainstream-watershed | 47.6 | 12 | 3.9 | 2 | 8.1 | 5.3 |
| Peakwatershed | 92.9 | 0 | 0 | 5.2 | 0 | 0 |
| PennyGulch-watershed | 95.7 | 2.0 | 0.5 | 0.5 | 0 | 0 |
| RoughGulch-watershed | 93.4 | 0 | 0 | 5.5 | 0 | 0 |
| SageCreek-watershed | 80.8 | 1.7 | 3.1 | 1.1 | <1 | 7.5 |
| SulphurCreek-watershed | 92.5 | 0.6 | 0.5 | 2.3 | <1 | 1.5 |

| | | | | | | |
|---|---|---|---|---|---|---|
| Unnnamed-Tribwatershed | 38.7 | 36.0 | 12.1 | 5.3 | 2.4 | 0 |
| Unnamed-Creekwatershed | 57.8 | 32.6 | 5.7 | 0.8 | <1 | <1 |

Land Cover Classification types derived from NLCD (2019)

**Appendix C:** *Additional Precipitation Figures*

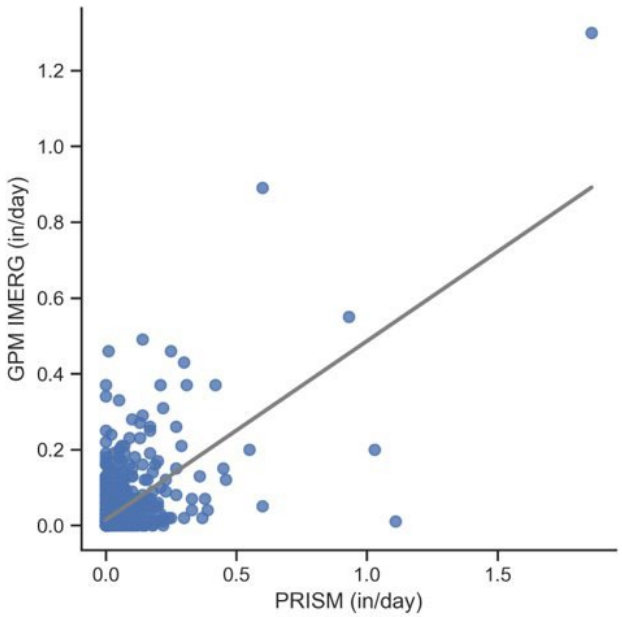


*Figure C1.* GPM IMERG daily precipitation averages against PRISM daily precipitation averages from January 2019 to October 2021 ($R^2 = 0.40$).

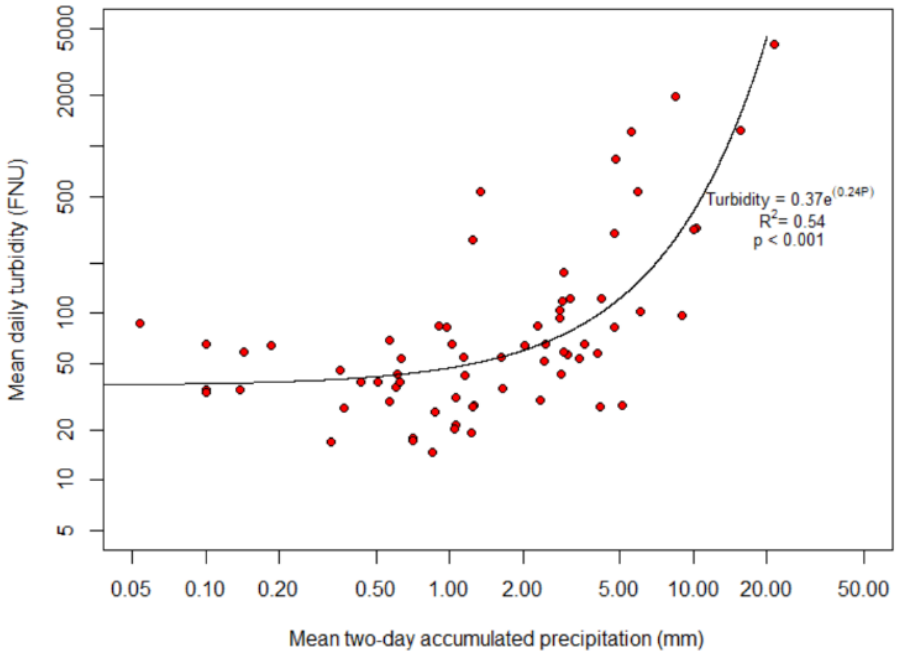


*Figure C2.* "Preliminary empirical relationship between mean two-day accumulated precipitation and mean daily turbidity measured at USGS Streamflow gaging station 06283995. Data were taken for the summer of 2019 for days when total measured rainfall depth exceeded 0.01 mm" (Alexander 2021).